

Excellence in Chemistry Research

Announcing our new flagship journal

- Gold Open Access
- Publishing charges waived
- Preprints welcome
- Edited by active scientists



Meet the Editors of *ChemistryEurope*



Luisa De Cola

Università degli Studi
di Milano Statale, Italy



Ive Hermans

University of
Wisconsin-Madison, USA



Ken Tanaka

Tokyo Institute of
Technology, Japan

Amine Functionalization Within Hierarchically-Porous Zeotype Framework for Plasmonic Catalysis over PdAu Nanoparticles

Priyanka Verma,^{*,[a, b, c]} Kohsuke Mori,^[a] Yasutaka Kuwahara,^[a] Maela Manzoli,^[d] Sara Morandi,^[e] Choji Fukuhara,^[c] Robert Raja,^{*,[b]} and Hiromi Yamashita^{*,[a]}

Plasmonic catalysis has revealed improved product yield and selectivity in various chemical transformation reactions over the past decade. In this report, the effect of tertiary amine (-NR₃) functionalization on the surface of hierarchically-porous zeotype (HP-AIPO-5) materials to enhance the plasmon-mediated catalysis, utilizing a combination of the plasmonic antenna (Au) and catalytic reactor (Pd) nanoparticles (NPs) was investigated. The catalysts have been characterized using enhanced techniques such as HAADF-STEM, FT-EXAFS, and probe-based FT-IR to reveal the proximity and interaction between bimetallic NPs, and thermal stability of amines in the presence of Au or PdAu NPs. Interestingly, a four-fold enhancement in the Suzuki-Miyaura coupling reaction product yield was obtained over PdAu/HP-AIPO-5-NR₃ when compared with the analogous

plasmonic catalyst with no amine functionalization under visible light irradiation. A range of amines were functionalized and their influence in the nucleation, uniform growth and stabilization of catalytic active site (Pd) and formation of electron-rich species under visible light irradiation has also been investigated. The presence of tertiary amine in the nanostructured catalyst enhanced the turnover number (TON) significantly under light irradiation conditions in comparison to dark conditions. This study provides an enriched understanding of plasmon-driven chemistry, where the maximized reaction rate enhancement requires the existence of active metal species and the formation of electron-enriched species under light irradiation conditions.

Introduction

The collective oscillation of conductive electrons in noble metal nanostructures^[1–3] (Ag, Au, or Cu) by the light irradiation of suitable wavelength is widely known as localized surface plasmon resonance effect (LSPR).^[4] It has already been evidenced that upon excitation, the generation of hot charge carriers by the noble metal nanoparticles (NPs) can drive various chemical reactions, for example, hydrogenation, dehydrogenation and organic synthesis.^[5] The high energy charge carriers, such as hot electrons and hot holes, are generated on the surface by the direct interband, intraband, or the geometry-assisted decay of LSPRs.^[6] The plasmonic metal NPs are coupled with active metal species to develop unique heterostructures,

which can influence the efficiency of employing green chemistry in organic synthesis.^[1]

In the last decade, our group has established the concept, design, and development of various plasmonic metal NPs (Ag and Au-based) in combination with Pd, Pt, Ru, Ni, or Co species.^[7–13] In this report, we have investigated the promotional effect of amine group functionalization on the enhancement of reaction rate under visible light irradiation conditions. Furthermore, the use of zeotype materials as a support has been utilized to study the plasmon-mediated catalysis of PdAu NPs, which has not been reported so far.

Zeolites have widespread applications in several industrial applications because of their exceptional properties, robust nature, and easily tunable catalytic properties. However, the


[a] Dr. P. Verma, Prof. K. Mori, Prof. Y. Kuwahara, Prof. H. Yamashita
Division of Materials and Manufacturing Science, Graduate School of Engineering
Osaka University
2-1 Yamadaoka, 565-0871 Suita, (Japan)
E-mail: yamashita@mat.eng.osaka-u.ac.jp
verma.priyanka@shizuoka.ac.jp

[b] Dr. P. Verma, Prof. R. Raja
School of Chemistry
University of Southampton
SO17 1BJ Highfield (United Kingdom)
E-mail: r.raja@soton.ac.uk

[c] Dr. P. Verma, Prof. C. Fukuhara
Department of Applied Chemistry and Biochemical Engineering
Faculty of Engineering
Shizuoka University
3-5-1, Johoku, Naka-ku, 422-8561 Hamamatsu, Shizuoka (Japan)

[d] Prof. M. Manzoli
Department of Drug Science and Technology
NIS Center and INSTM Reference Center
University of Torino
Via P. Giuria 9, 10125 Torino (Italy)

[e] Dr. S. Morandi
Department of Chemistry
NIS Center and INSTM Reference Center
University of Torino
Via P. Giuria 7, 10125 Torino (Italy)

 Supporting information for this article is available on the WWW under <https://doi.org/10.1002/cctc.202201182>

presence of micropores restricts the diffusion of substrate molecules, decreasing the overall rate of reaction. The zeotype support material developed in this study uses a soft-templating approach to generate mesopores, which are interconnected with the micropores, to generate hierarchically porous (HP) aluminophosphates (HP-AIPO-5).^[14,15] This facilitates the development of higher surface area materials with isolated and accessible active sites that could be located within the mesopores to aid stability and overcome the mass-transfer limitations.^[16] The preservation of porosity after NPs deposition and reaction rate enhancement with hierarchical architectures in comparison to microporous AIPOs has already been established in our previous report.^[17]

The preparation of plasmonic antenna (Au NPs) in combination with catalytic active (Pd) has become a popular combination to investigate the plasmon-mediated catalytic reaction because of the high stability, strong plasmonic absorption of Au and superior catalytic activity of Pd NPs.^[18–20] The plasmonic enhancement of light absorption in Au is caused by the resonant excitation of incoming light irradiation and free electrons present in the metal.^[21] In this study, hierarchically porous support material was used to tune the diameter of plasmonic Au NPs and the efficacy of Pd NPs on the Au surface. This has been achieved by a control experiment with various amine group functionalization on the surface of HP-AIPO-5. In general, Au NPs tend to aggregate to form larger-sized particles; therefore, the use of hierarchically porous support material was adopted to tune the size of NPs less than 10 nm. To test the efficacy of our prepared catalysts, we employed the Suzuki-Miyaura coupling reaction to study the difference in the catalytic performance ability in dark and under visible light irradiation conditions.^[22] The combination of the plasmonic antenna (Au) and chemical reactor (Pd) in the Suzuki-Miyaura coupling reaction has been reported to display enhanced product yields under visible light irradiation conditions. Han et al. have recently reported the design of Pd–Au NPs supported on ZrO₂ with a SiO₂ layer between Au and Pd NPs, displaying a biphenyl product yield = 63.1%.^[23] Koeckelberghs's group reported a 57% product yield of 4-methylbiphenyl utilizing Fe₃O₄/Au/PEG/Pd nanocatalyst.^[24] A list of recently published Pd-based plasmonic catalytic systems has been tabulated (Table S1) to understand the current scenario in the efficiency of product formation. In this report, to further increase the catalytic performance of the Suzuki-Miyaura coupling reaction under solar light irradiation, we have experimented with the use of surface-functionalized zeotype materials with the addition of different kinds of amines, for example, primary (–RNH₂), secondary (–NHR₂), tertiary (–NR₃) groups and the presence of one, two and three nitrogen atoms containing amines. A plausible mechanism of catalytic activity enhancement for plasmon-mediated Suzuki-Miyaura coupling reaction under visible light irradiation has been proposed to correlate the promotional effect of amine groups with the obtained plasmon-mediated catalytic performances under visible light irradiation.

Results and Discussion

To verify the stability of the amine on HP-AIPO-5-NR₃, i.e., the functionalization that resulted in the most efficient ion influencing the reaction rate under visible light irradiation, FT-IR spectra were collected during outgassing at increasing temperature (Figure 1).

Bands characteristic of the amine^[25] confirming the successful functionalization appear at: (i) 2970 and 2885 cm^{−1} (–CH₃ stretching asym and sym, respectively), 1460 and 1380 cm^{−1} (–CH₃ bending asym and sym, respectively); (ii) 2932, 2802 and 1493 cm^{−1} (–CH₂– stretching asym and sym, respectively and bending). In addition, other bands were observed at: (i) 3025 cm^{−1} (stretching of –CH=); (ii) 3085 and 1420 cm^{−1} (=CH₂ asym stretching and bending, respectively); (v) 1640 and 1600 cm^{−1} (stretching of C=C). These features, already present at room temperature, reveal the formation of C=C double bonds on the amine chains during the synthesis. Moreover, C–C, C–O and C–N stretching modes of the amine contribute to the overall absorption in the 1500–1300 cm^{−1} interval. All bands do not undergo significant changes by increasing the temperature, which reveals the thermal stability of the amine up to 573 K.

The thermal stability of the amine did not change in the presence of Au or PdAu NPs, as revealed by similar experiments on Au/HP-AIPO-5-NR₃ and PdAu/HP-AIPO-5-NR₃ catalysts (Figure S1 and S2, respectively). Moreover, the effect of the addition of either Au or PdAu NPs on the functionalization with NR₃ was also put in evidence by comparing the FT-IR spectra of HP-AIPO-5-NR₃, Au/HP-AIPO-5-NR₃ and PdAu/HP-AIPO-5-NR₃ outgassed at 573 K, as shown in Figure 2. As a matter of fact, bands related to the presence of amine (highlighted by vertical bars in the Figure 2) were observed on all functionalized samples, but the intensity of the absorption varied in the presence of the metal NPs. In particular, the intensity followed the order: HP-AIPO-5-NR₃ > Au/HP-AIPO-5-NR₃ > PdAu/HP-AIPO-5-NR₃, resulting in a lower amount of surface amine when metals are added. This feature is well evident in the 3200–2750 cm^{−1} range, whereas the 1720–1530 cm^{−1} range was not informative due to

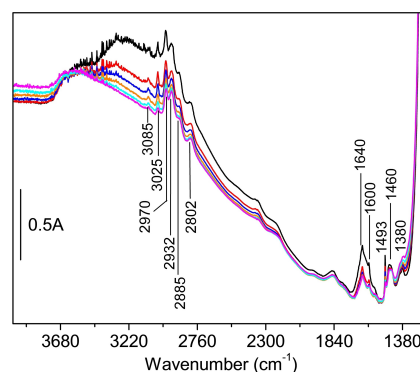


Figure 1. FT-IR Absorbance spectra of HP-AIPO-5-NR₃ under outgassing at room temperature (black line), 373 K (red line), 423 K (blue line), 473 K (orange line), 523 K (cyan line), and 573 K (magenta line).

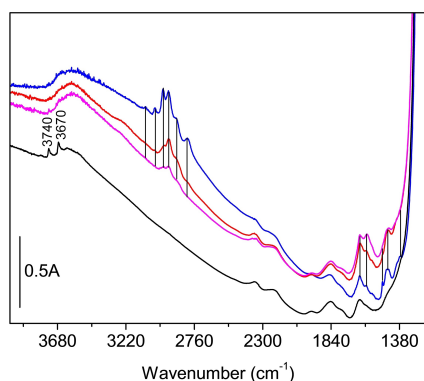


Figure 2. FT-IR Absorbance spectra of HP-AIPO-5-NR₃ (blue line), Au/HP-AIPO-5-NR₃ (red line), PdAu/HP-AIPO-5-NR₃ (magenta line), and HP-AIPO-5 (black line) after outgassing at 573 K.

the variation in the refractive index of the AIPO-5 upon metal addition.

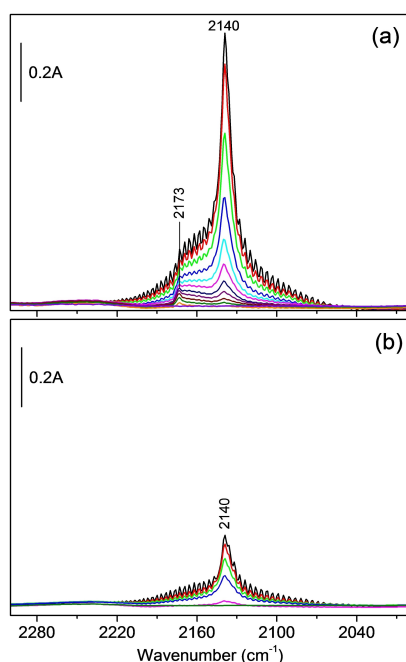


Figure 3. FT-IR difference spectra of CO adsorbed at 77 K upon increasing pressure up to 50 mbar on HP-AIPO-5 (a) and HP-AIPO-5-NR₃ (b) after outgassing at 573 K. The spectra have been normalized to the optical density of the pellets.

Two narrow peaks at 3740 and 3670 cm⁻¹, assigned to the stretching of free Al-OH and P-OH, respectively,^[26] were observed in the spectrum of HP-AIPO-5 after outgassing at 573 K (black line in Figure 2). These peaks were not detected for the functionalized materials (blue, red and magenta lines), indicating that the presence of Al-OH and P-OH groups assists in the anchoring of the amine.

To get further insights on the functionalization, CO adsorption at 77 K on HP-AIPO-5 without and with amine was performed and reported in Figure 3a and b, respectively. Increasing doses of CO on HP-AIPO-5 (Figure 3a) produced a sharp peak at 2140 cm⁻¹ with a component at 2173 cm⁻¹, assigned to liquid-like CO inside the pores and to CO in interaction with P-OH groups, respectively.^[27] As for HP-AIPO-5-NR₃ (Figure 3b), it is worthy of note that (i) the latter absorption was not observed at all and (ii) the intensity of the band related to liquid-like CO inside the pores was markedly decreased. These results confirmed on one hand that the P-OH groups were engaged in the functionalization and, on the other hand, that the presence of the amine reduced the pore accessibility. This last finding was corroborated by the textural characterization reported below. The textural properties of hierarchically-porous zeotype materials before and after amine functionalization and metal NPs deposition were studied by N₂ physisorption at 77 K (Figures S3 and S4).

Table 1 enlists the BET-specific surface area (SSA), pore volume and SSA of micro and mesopores of all samples. The type IV isotherm with a pronounced knee in the bare support framework confirmed the presence of mesoporous structure along with micropores (Figure S3a). The presence of the amine markedly decreased the microporosity, as shown by the less evident knee in Figure S3a and by the particularly decreased micropore volume reported in Table 1. More in detail, the microporosity abatement upon functionalization concerned micropores with sizes smaller than 1 nm (Figure S4a). Also, a slight decrease in the mesopore volume was observed along with the formation of a microporosity between 1 and 2 nm (Figure S4b). This suggested that the surface of mesopores was covered by amine producing a decrease in size. The addition of Au NPs further slightly decreased the SSA, given a similar pore distribution (Table 1 and Figure S4b). Conversely, the subsequent Pd addition induced an increase in the SSA with respect to the functionalized support, as displayed by the partial recovery of microporosity < 1 nm (Figure S4a) which indicated the involvement of the amine in anchoring Pd NPs within the mesopores of HP-AIPO-5-NR₃. Finally, the results obtained for PdAu/HP-AIPO-5, demonstrated that the metal deposition

Table 1. Textural properties and particle size of the prepared catalysts.

Sample	BET surface area [m ² g ⁻¹]	Total pore volume [cm ³ g ⁻¹]	Microporous pore volume [cm ³ g ⁻¹]	Mesoporous pore volume [cm ³ g ⁻¹]	SSA _{meso} [m ² g ⁻¹]	SSA _{micro} [m ² g ⁻¹]
HP-AIPO-5	240	0.187	0.077	0.110	69	144
HP-AIPO-5-NR ₃	86	0.109	0.019	0.090	39	24
Au/HP-AIPO-5-NR ₃	73	0.112	0.016	0.096	30	24
PdAu/HP-AIPO-5-NR ₃	93	0.119	0.026	0.093	32	44
PdAu/HP-AIPO-5	113	0.130	0.039	0.091	24	81

Sample	Al	P	Au	Pd	C	H	N
HP-AIPO-5	19.7	19.3	–	–	<0.1	1.1	<0.1
HP-AIPO-5-NR ₃	17.9	16.9	–	–	7.7	1.5	0.6
Au/HP-AIPO-5-NR ₃	19.7	18.8	2.1	–	6.0	1.1	0.6
PdAu/HP-AIPO-5-NR ₃	19.6	19.1	1.9	0.3	4.0	1.0	0.5
PdAu/HP-AIPO-5	20.1	21.2	1.6	0.1	<0.1	0.7	<0.1

affected in lower extent both surface area and porosity as well (Table 1).

The elemental analysis by ICP and CHN analysis revealed the exact weight % loadings of Al, P, C, H, N and metal NPs of Au and Pd as shown in Table 2. The Al and P content was maintained at approximately 20 wt.% each in all samples. The N content of HP-AIPO-5 before functionalization was found to be less than 0.1% and with the amine functional group, 0.63% of N content was obtained in HP-AIPO-5-NR₃. No significant change in the N content was observed after loading with PdAu bimetallic NPs on HP-AIPO-5-NR₃. The use of different amines led to the varied contents of nitrogen amounts as enlisted in Table S3. The highest nitrogen content was found to be in HP-AIPO-5-Amine-1 (4.0%), because of its simple linear structure, leading to easy functionalization on the support framework. Amine-3 nitrogen content on the support framework was 3.03% which was due to the presence of multiple nitrogen atoms. Amine-4 displayed the least nitrogen content (0.63%), caused by the steric hindrance of alkyl groups around the nitrogen atoms in tertiary amines (-NR₃). A relative decrease in the CHN content was observed after PdAu deposition. However, the stability of amine group functionalization on the support surface was affirmed by FT-IR spectroscopy as already discussed and X-ray photoelectron spectroscopy (XPS) analysis (*vide infra*).

The amine group functionalization, bimetal NPs deposition and even treatment with higher temperatures for metal precursor reduction did not affect the crystallinity and phase purity of materials as shown in Figure 4a. The presence of crystalline Au in the cubic phase was affirmed in the XRD pattern shown in Figure 4b, where (111), (200), (220) and (311) planes have been highlighted with black points (JCPDS file number 00-001-1172). However, the presence of crystalline Pd NPs was not detected, possibly due to the low Pd loading.

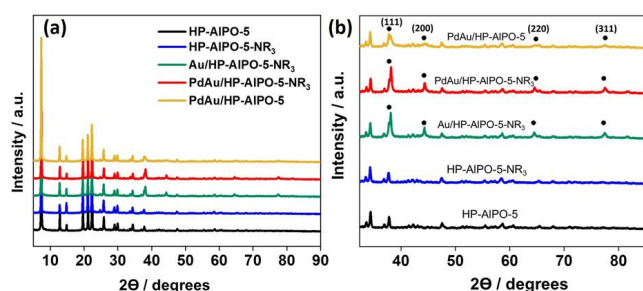


Figure 4. (a) XRD patterns of the prepared catalysts (b) magnified XRD pattern to assign the presence of Au NPs.

The optical absorption arising from the amine groups and the LSPR effect of Au NPs was measured by UV-vis spectroscopy, as shown in Figure 5. No absorption bands were observed in the HP-AIPO-5 support, which ascertains the suitability of this support material for studying the effect of plasmonic absorption by metal NPs. The modification with amine groups displayed a complex and broad absorption in which multiple peaks can be discerned in the 200–350 nm range, which is a characteristic feature for amino functional groups.^[28] The immobilization of Au and PdAu NPs did not affect the absorption arising from amine functional groups. An intense plasmonic band of Au NPs was observed at 532 nm. After Pd NPs deposition, the plasmon band position was preserved at 529 nm.^[9] However, a decrease in intensity of the plasmonic absorption was observed for PdAu/HP-AIPO-5-NR₃, evidencing the possible close contact of Pd on the surface of Au. Figure S5 shows the absorption spectra of remaining PdAu/HP-AIPO-5-Amine-x (x=1, 2 and 3). It was observed that -NR₃ (Amine-4) caused the least intensity in bimetallic nanocatalyst, implying the highest surface coverage of Au NPs.

The particle size and morphology of bimetallic NPs in PdAu/HP-AIPO-5-NR₃ were evidenced by performing HAADF-STEM (high-angle annular dark-field scanning transmission electron microscopy) measurements, as shown in Figure 6. The elemental mapping of Au and Pd and the presence of other elements in the support framework (Al and P) were also evidenced. The support framework comprises Al and P tetrahedral moieties bonded with oxygen; the mapping results confirm the uniform dispersion. The amine functionalization was also confirmed by the presence of uniformly distributed nitrogen (N) atoms on the support framework. The HAADF-STEM focuses on a single NP-sized 24 nm Au core covered with a Pd shell on the surface, verifying the proof-of-concept of the synthetic strategy of bimetallic NPs.

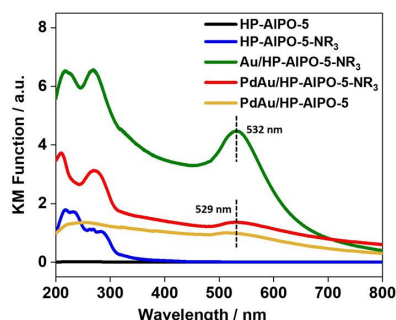


Figure 5. UV-vis spectra of the prepared catalysts.

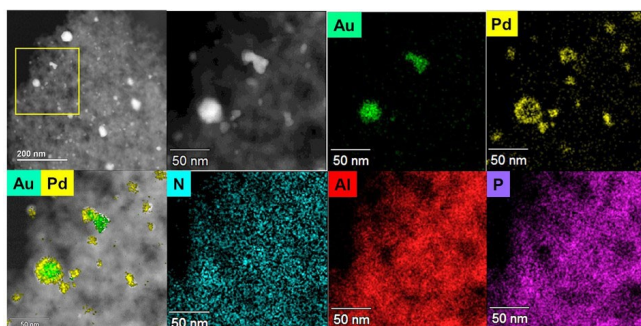


Figure 6. HAADF-STEM image of PdAu/HP-AIPO-5-NR₃ along with elemental mapping of Au, Pd, N, Al, and P.

The average particle size of Au/HP-AIPO-5-NR₃, PdAu/HP-AIPO-5-NR₃, and PdAu/HP-AIPO-5 were evaluated by TEM measurements (Figure S6) and found to be $d_m = 7.5 \pm 3.8$ nm, 10.1 ± 3.9 nm and 6.9 ± 3.9 nm, respectively. The increase in the average diameter for PdAu/HP-AIPO-5-NR₃ with respect to Au/HP-AIPO-5-NR₃ confirmed the efficient deposition of Pd on Au NPs.

From ICP analysis, a drastic change in the dispersion and the amount of Pd loading on the surface of HP-AIPO-5 was observed in the presence and absence of an amine functional group. The loading of Au amount remained almost the same in all cases. Different kinds of amines (for example, primary, secondary, and tertiary) can affect the nucleation and covalent anchoring of Pd NPs within the mesopores of HP-AIPO-5. The obtained results suggest that primary (Amine-1; -NH₂) and tertiary amines (Amine-4; -NR₃) were most efficient in achieving higher loadings of Pd content (Table S2).

X-ray absorption spectroscopy (XAS) is an essential tool for gathering spectroscopic information based on the electronic structure and the atomic configuration geometry of catalysts in their local environment. The oxidation state and coordination environment of Au and Pd metal NPs were studied by analyzing X-ray absorption near edge structure (XANES) and Fourier transform-extended X-ray absorption fine structure (FT-EXAFS) spectra. Figure 7a,c shows the Au L_{III}-edge XANES and FT-EXAFS spectra of prepared catalysts and their comparison with reference Au foil and the precursor solution. In XANES spectra, a decrease in the intensity of the white line for bimetallic PdAu/HP-AIPO-5 and PdAu/HP-AIPO-5-NR₃ in comparison to Au foil and Au/HP-AIPO-5 confirms the possible interaction and charge transfer between the two metals.^[29] In particular, the decreased intensity evidence the filling of electron density of unoccupied 5d states in bimetallic PdAu NPs, corresponding to the electronic transition from 2p to 5d.^[30,31] The FT-EXAFS spectra of monometallic and bimetallic species displayed an intense peak at 2.5 Å, similar to Au foil and completely different from the peak of HAuCl₄ precursor solution at 1.9 Å. This confirms the formation of Au NPs in a metallic oxidation state.

Similarly, the state of Pd was confirmed by Pd K-edge XAS measurements, as shown in Figure 7b, d. The reference samples used were Pd foil and Pd(OAc)₂ precursor solution. The

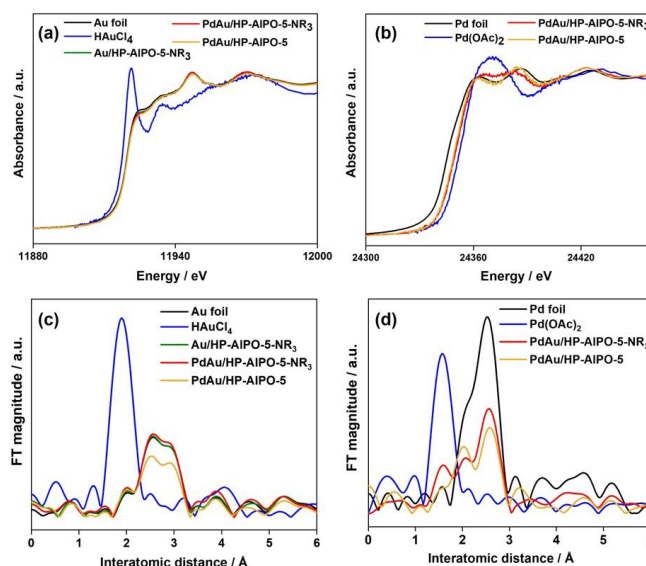


Figure 7. XAS spectra of PdAu bimetallic NPs deposited on HP-AIPO-5. XANES spectra of (a) Au-L_{III} edge, (b) Pd k-edge and FT-EXAFS spectra of (c) Au L_{III}-edge and (d) Pd k-edge.

significant component of Pd NPs was in Pd⁰ oxidation state, as seen from an intense peak observed at 2.5 Å in the FT-EXAFS spectra. The XANES spectra also depict a similar curve to that of Pd foil. The shift of peak for bimetallic NPs towards lower energy attributes to some degree of reduction. The metal oxidation state with different amine-functionalized support was also confirmed, as summarized in Figure S7. As expected, a decreased white line intensity peak was obtained for bimetallic species, and the presence of metallic NPs was confirmed.

Furthermore, the XPS analysis was carried out to study the possible interaction and oxidation state of metal NPs. The C1s peak at B.E. = 284.8 eV was used to calibrate the obtained data of all the samples. The grafting of amino groups on the surface of the support framework was already confirmed by FT-IR spectroscopy, CHN analysis, and also by the presence of 'N' atoms in the HAADF-STEM elemental mapping analysis. The N 1s XPS spectra of the amine-functionalized support framework displayed a peak at 401.9 eV and 398.8 eV attributing the confirmation of the presence of nitrogen atoms as amines (Figure S8). No significant difference in the N1s spectra was observed after step-wise deposition of Au and Pd NPs on the support, confirming the successful retainment of -NR₃ groups. Figure S8 also includes the N1s spectra of the re-used sample, which shows a similar peak with a slight shift in the B.E. towards a higher value due to the electron donation effect from amine groups to metal NPs.^[32,33] Figure 8 displays the Au 4f and Pd 3d XPS spectra of monometallic and bimetallic PdAu samples before and after amine functionalization. The binding energy (B.E.) of Au and Pd in all the prepared samples confirmed the valence of Au⁰ and Pd⁰ in the metallic state, and peaks arising from Au⁺, Pd²⁺, and other oxide species were not observed. As for the Au/HP-AIPO-5-NR₃ sample, the B.E. of Au 4f was shifted towards a lower value (83.5 eV) compared with

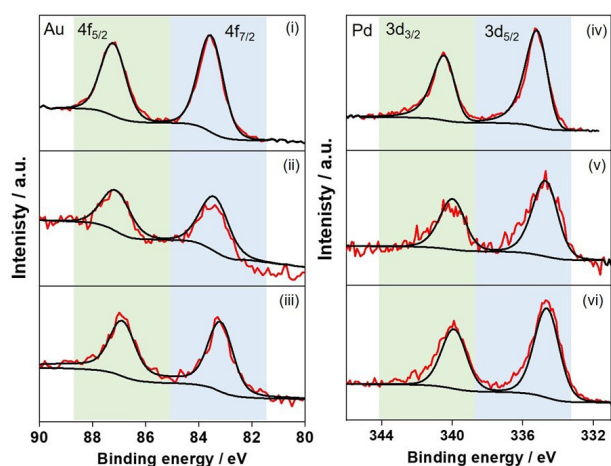


Figure 8. The XPS spectra of monometallic and bimetallic catalysts. Au 4f for (i) Au/HP-AIPO-5-NR₃, (ii) PdAu/HP-AIPO-5-NR₃, (iii) PdAu/HP-AIPO-5 and Pd 3d spectra of (iv) Pd/HP-AIPO-5-NR₃, (v) PdAu/HP-AIPO-5-NR₃ and (vi) PdAu/HP-AIPO-5.

that of a standard value (Au⁰: 84.0 eV), indicating the formation of more electron-rich Au with amine functionalization. Upon comparing the Au 4f XPS spectra in Au/HP-AIPO-5-NR₃ (B.E. = 83.5 eV) and PdAu/HP-AIPO-5-NR₃ (B.E. = 83.4 eV), the B.E. shifted towards a lower value for the bimetallic sample. This can be inferred from the charge transfer from Pd to Au due to the electronegativity difference between the two elements (χ_{Au} : 2.54, χ_{Pd} : 2.2). A similar trend was observed in PdAu/HP-AIPO-5 without amine functionalization. However, the Pd 3d XPS peaks of PdAu/HP-AIPO-5-NR₃ (334.7 eV) was also found to be shifted towards a lower B.E. value when compared with that of standard Pd⁰ NPs (335.0 eV), which is indicative of the electron donation effect from Brønsted basic tertiary amine species to the Pd NPs. The B.E. values of prepared catalysts, the standard peaks along with their corresponding shifts has been tabulated (Table S4), as observed in the XPS spectra. The obtained shifts suggests the alloying effect between the bimetallic NPs, as already evidenced in the TEM analysis. Overall, these observed shifts in the B.E. confirm the formation of electron-rich metal species and the existence of strong metal-functionalized support interactions.

Plasmonic catalysis: Suzuki-Miyaura coupling reaction

To test the applicability of the prepared plasmonic catalysts, the Suzuki-Miyaura coupling reaction was selected as a model reaction to study the influence of amine functionalization and visible light irradiation on the prepared catalysts. The Pd-catalyzed Suzuki-Miyaura coupling is one of the powerful and convenient reactions to carry out the synthesis of biaryls by carbon-carbon bond formation, an essential structural unit found in natural products, pharmaceuticals, and advanced materials.^[34]

The reaction was carried out in the presence of a weak base, K₂CO₃, and ethanol as the solvent, at room temperature in

the dark, and under visible light irradiation conditions ($\lambda > 420$ nm).

At first, the significance of the hierarchically-porous (HP) support framework was justified by comparing the reaction kinetics of microporous (MP) and HP support framework over PdAu/HP-AIPO-5 catalyst under visible light irradiation conditions. However, the MP support framework did not display any product yield, in dark or under light irradiation, due to diffusion limitations (Figure S9).^[17] The product yield of monometallic Au/HP-AIPO-5-NR₃ and Pd/HP-AIPO-5-NR₃ was 0% and 50%, respectively, under visible light irradiation, validating the 'Pd' NPs as the active site in this reaction (Figure S10).

Figure 9a displays different amine groups used for functionalization ranging from primary (Amine-1), secondary (Amine-2 and Amine-3), and tertiary groups (Amine-4) on the surface of the HP-AIPO-5 support framework. The optimization of the amount of tertiary amine group (Amine-4; NR₃) per gram of the support framework is shown in Figure 9b. It was observed that upon increasing the amount of amine from 0, 1 to 5 mmol on the surface of HP-AIPO-5 (1 g), the plasmon-mediated catalytic yield was found to enhance significantly from 17%, 60% to 70%, respectively. However, upon further increasing the amine content to 10 mmol, the catalytic activity drastically reduced to 10% under visible light irradiation conditions. Even extending the reaction time from 4 to 24 h, had no effect on increasing the catalytic performance. This confirmed the importance of having the optimized amount of amine groups on the HP-AIPO-5 as 5 mmol g⁻¹. Hence, it was selected as an optimized amount for the preparation of samples with other different amines. The reaction results in dark and visible light irradiation conditions with different amine groups, as shown in Figure 9c. It can be seen that Amine-4 (-NR₃) was found to be most efficient in enhancing the rate of a reaction under visible light irradiation. This can be attributed to the promotional effect of Brønsted basic sites, increasing the electron flux on the surface of Au NPs. The bulkier amines have been reported to be better ligands in enhancing the efficiency of the Suzuki-Miyaura coupling reaction because of electron donation and the formation of a stable intermediate.^[35] This phenomenon leads to the creation of electron-enriched Au under light irradiation conditions due to the generation of hot electrons by the Au LSPR effect. The enriched Au can efficiently make electrons available on the Pd surface under irradiation and adsorbed substrate molecules to form biphenyl, as discussed in detail in the mechanism section. Interestingly, the catalytic activities obtained in dark conditions did not affect the type of amine functionalization, indicating that sufficient electron flux is needed to drive the reaction forward.

Figure 9d displays the product yield enhancement with a ratio of TON in light and dark conditions. The enhancement percentage was highest for PdAu/HP-AIPO-5-NR₃, amongst all amines, due to the highest electron flux density of tertiary amines. It must be noted that although the presence of amine groups had a positive impact on enhancing the catalytic performance by providing sufficient electron density and basicity in the system, the catalytic reaction did not proceed in

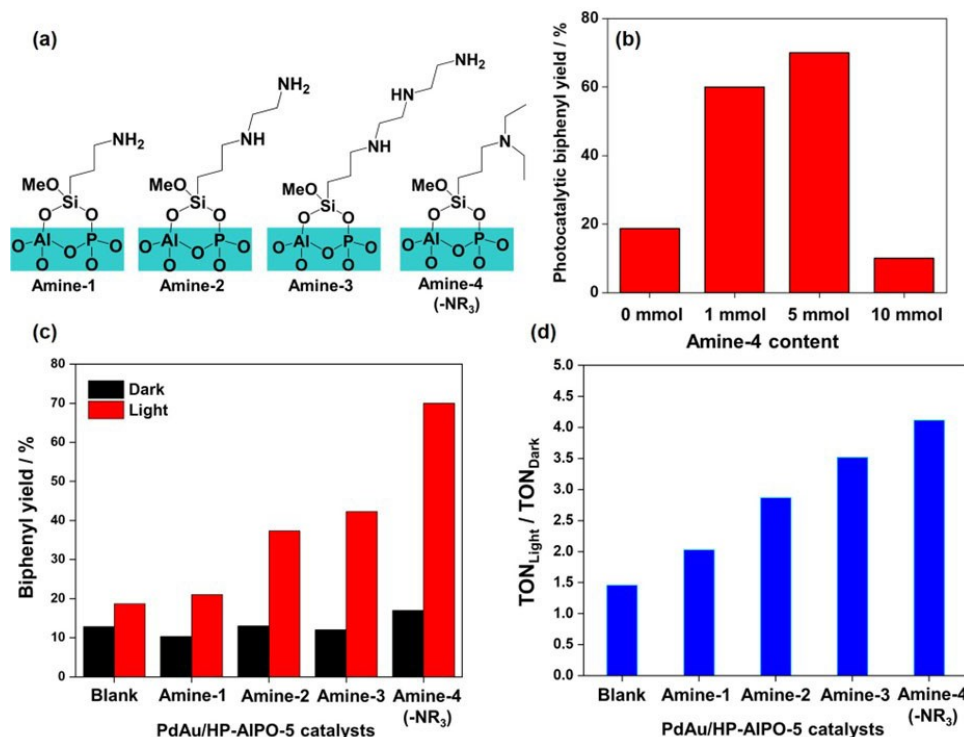


Figure 9. Plasmon-mediated Suzuki-Miyaura coupling reaction over PdAu/HP-AIPO-5 catalysts. (a) Different amine groups used for functionalizing HP-AIPO-5 support framework, (b) Optimization of amine content over PdAu/HP-AIPO-5-Amine-4 catalyst in the Suzuki-Miyaura coupling reaction under visible light irradiation, (c) Effect of different amine groups in the product yield in dark and under visible light irradiation and (d) A comparison of the ratio of TON obtained in light and dark conditions. Reaction conditions: catalyst (50 mg), phenylboronic acid (0.9 mmol), K₂CO₃ (0.9 mmol), Iodobenzene (1.0 mmol), ethanol (15 mL), visible light $\lambda > 420$ nm.

the absence of mild base K₂CO₃ over PdAu/HP-AIPO-5 and PdAu/HP-AIPO-5-NR₃ plasmonic catalyst.

To understand the working mechanism of LSPR, the effect of UV and visible light irradiation was studied during the photocatalytic reaction. It was observed that the combination of UV and visible light had a negative impact on the catalytic performance when compared with irradiating only visible light. A decrease in the catalytic reaction yield by 12% was observed when UV was combined with visible light. This observation is due to the decrease in the efficacy of light photons on visible-light sensitive Au NPs (Figure 10a). Our previous study observed

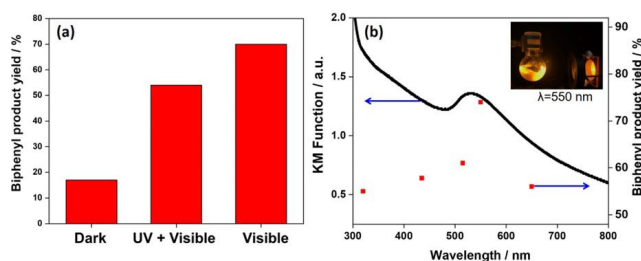


Figure 10. (a) Effect of using different filters on the product yield (b) Wavelength-dependent product yield over PdAu/HP-AIPO-5-NR₃ catalyst ($\lambda = 320, 435, 515, 550$ and 650 nm). Reaction conditions: catalyst (50 mg), phenylboronic acid (0.9 mmol), K₂CO₃ (0.9 mmol), Iodobenzene (1.0 mmol), ethanol (15 mL), visible light.

an opposite effect when UV and visible light irradiation enhanced the catalytic yield of plasmonic Ag NPs combined with UV-responsive single-site Ti-oxide moieties.^[11] To further confirm the effect of Au LSPR, the action spectrum of the PdAu/HP-AIPO-5-NR₃ catalyst was studied by irradiating light of different wavelengths according to the absorption spectrum ($\lambda = 320, 435, 515, 550$, and 650 nm). Interestingly, the product yield varied when the reaction kinetics was compared in dark and light irradiation of different wavelengths (Figure 10b). As expected, the highest catalytic performance (74% yield) was observed at $\lambda = 550$ nm at an absorption peak maximum, further confirming the reaction rate enhancement is due to the LSPR effect of Au NPs, assisted by Pd and Brønsted basic amine functional groups. This product yield was even higher than the product yield under visible light irradiation conditions.

The recycling ability and stability of the prepared catalyst were also investigated, as shown in Figure S10. A relatively stable catalytic performance was observed when the re-used catalyst was employed in the plasmonic catalysis (yield = 65%). The re-used catalyst was then characterized by ICP, UV-vis, XPS, and XRD to confirm the preservation of the support framework and stability of metal NPs. ICP analysis displays a slight change in the metal loadings (by ~ 0.09 wt.% in the case of Pd) in the re-used catalyst, confirming that there is minimal leaching effect when employing the re-used catalyst for plasmonic catalysis. The crystalline framework in XRD confirmed the

preservation of the HP-AlPO-5 framework after the reaction (Figure S11). Figure S11 also shows the UV-vis spectra of the re-used sample, which displayed a slight decrease in the intensity of the plasmon peak at the 500 nm wavelength region. This could be due to the surface adsorption of reaction substrate molecules which interfere with the light absorption ability of metal NPs. It was further evidenced by measuring the XPS spectra of the PdAu/HP-AlPO-5-NR₃-reused sample. Upon comparing the C1s peak of the fresh and re-used sample, different carbon species arising from the latter were observed, as shown in Figure S12.

The preliminary substrate scope of the reaction was tested using a bromobenzene reactant instead of iodobenzene. The product yield of 30% over PdAu/HP-AlPO-5-NR₃ was obtained under visible light irradiation, displaying its applicability with other substrates. The prepared catalysts were also active in the ammonia borane dehydrogenation reaction. A similar trend in the enhancement of catalytic activity with amine group functionalization was observed in the dark and under visible light irradiation conditions.

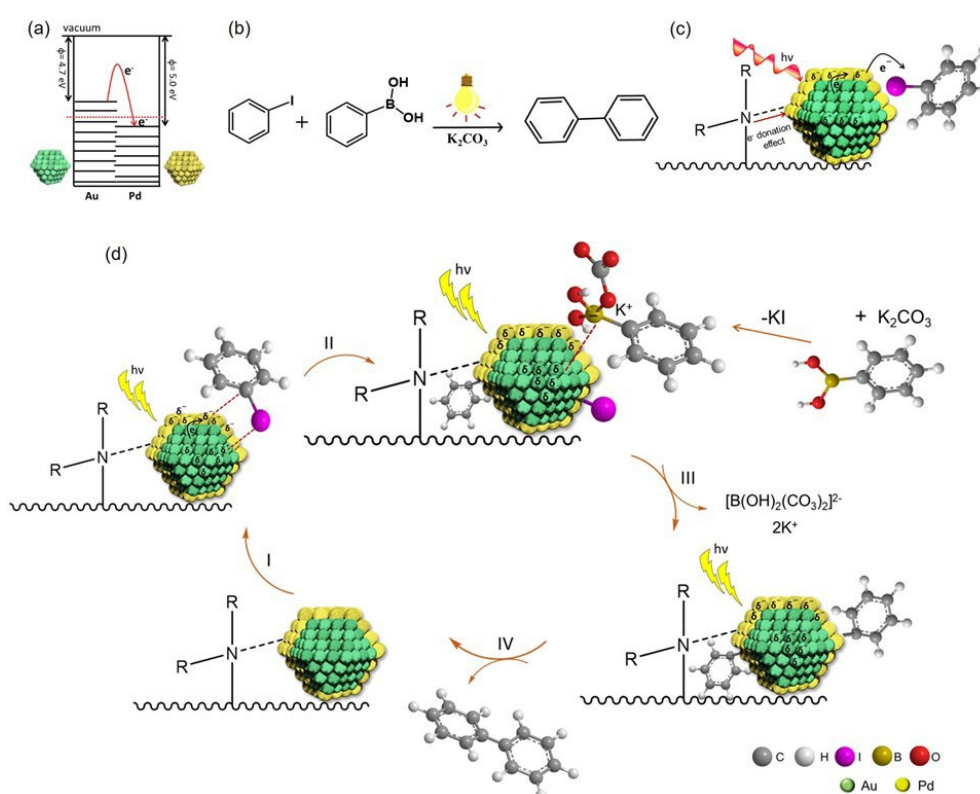
Effect of amine groups in the creation of active sites

The promotional effect of Brønsted basic amine groups, in enhancing the catalytic performance in Suzuki-Miyaura cou-

pling reactions, has been widely reported in the literature.^[35,36] The presence of amine groups assists in creating more synergistically active sites for improving the activation of reactant (iodobenzene) molecules. In addition, the uniform deposition of amino groups on the zeotype framework provides better stability due to the additional interaction with PdAu NPs.^[37] It has also been extensively researched that amino groups offer a platform for the nucleation, growth, and uniform dispersion of Pd NPs.^[38–40] The formation of coordinated covalent bonds between Pd and amino groups (also shown in Scheme 1) display their efficacy in acting as stabilizers and the homogenous dispersion of ultrafine Pd NPs.

To confirm the effect of nucleation and growth of Pd NPs, we performed a control experiment in which the deposition of the same target amount (1.0 wt.%) of Pd NPs was carried out through the same preparation process on the Au/HP-AlPO-5 framework in the presence and absence of amine groups. ICP analysis was employed to analyze the prepared catalyst's exact loaded amounts of Pd. It was observed that amine-free support could anchor only 0.09 wt.% of Pd and in the presence of amine groups, as high as 0.75 wt.% of Pd loading could be achieved (Table S2). This result reveals that the amine functionalization can stabilize the anchoring of Pd NPs by forming a coordinative covalent bond.

Interestingly, the Pd content was found to vary upon changing the type of amine from primary, secondary and



Scheme 1. A plausible mechanism for plasmon-mediated Suzuki-Miyaura coupling reaction under visible light irradiation. (a) electron transfer from Au to Pd, (b) scheme of catalytic reaction in this study, (c) illustration of charge separation in Au and Pd under light irradiation condition and interaction with iodobenzene substrate and (d) plausible mechanistic pathway in the Suzuki-Miyaura coupling reaction under visible light irradiation condition.

tertiary amine. The Pd loading amount did not correlate with the amount of nitrogen content and type of amines utilized for functionalization on the support framework. The amount of Au did not change in all catalysts, irrespective of the presence or absence of amine groups.

The unique interaction between the Pd and amine groups in combination with plasmonic Au played a crucial role in achieving superior photocatalytic performances and controlling the plasmon-mediated catalytic response. The modulation of electronic structure (evidenced by XPS analysis) and plasmonic absorption (UV-vis) can also be tuned by controlling the type of amine used for functionalization. These factors will ultimately affect the formation of ultrafine NPs and their catalytic performance. Theoretical and spectroscopical measurements have also proved that the bonding of metal NPs (especially Au or Pd) with electron-donating molecules (such as amines or pyridines) can lead to the formation of small-sized electron-rich metal clusters with enhanced catalytic activities.^[41] In addition, bulky ligands in tertiary amine might be responsible for improving the efficiency of the Suzuki-Miyaura coupling reaction.^[35]

A plausible mechanism for enhancing the photocatalytic activity in the Suzuki-Miyaura coupling reaction over PdAu NPs immobilized on an amine-functionalized HP-AIPO-5 framework has been proposed. Under visible light irradiation, the hot electron generation occurs on the plasmonic antenna 'Au' NPs. These hot electrons are then quickly transferred to the surface deposited catalytically active 'Pd' NPs.^[42-44] The binding between Au core and Pd NPs, as confirmed by the HAADF image and XPS characterization, allows for the efficient charge transfer between the two species.^[45] This electron transfer is feasible because of the Fermi energy level positioning with a work function value of 4.7 and 5.0 eV for Au and Pd, respectively (Scheme 1a).^[5] The substrate for the model test reaction in this study is iodobenzene and phenylboronic acid (Scheme 1b). The hot electrons migrating from the surface of Au to Pd can assist in the elongation and further cleavage of the C-I bond, as depicted in Scheme 1c.

Furthermore, the electron donation effect from the Brønsted base amine sites assists in enriching the electron density on the surface of Pd. Xiao et al. have employed DFT calculations to evidence the C-X bond elongation from 0.21 nm to 0.30 nm after hot electron injection from Au-Pd alloy NPs under visible light irradiation conditions.^[46] Feng et al. have also recently evidenced the hot electron-induced Suzuki-Miyaura coupling reaction by surface-enhanced Raman scattering (SERS) spectroscopic analysis over Au@Pd NPs.^[47] The transfer of hot electrons to the aryl-X was evidenced by the decrease in the intensity of ν_{C-X} bond in the SERS spectra (X = halide). The rate-determining step and the activation of substrate molecules, iodobenzene and phenylboronic acid, were enhanced due to the formation of electrons and holes on the PdAu NPs by the surface plasmon excitation under light illumination conditions.^[48] In our PdAu nanostructured catalysts, under visible light irradiation, the significant increase in the electron flux due to hot electrons and electron donation from the -NR₃ sites assist in the charge separation and adsorption of iodobenzene substrate on the surface of NP as shown in Step I (Scheme 1d). This oxidative

addition is also the rate-determining step in this reaction.^[49] Next step involves the reaction of phenylboronic acid with a base to form a boron-ate complex. The interaction of positive charge center of Au with the boron-ate complex is shown in in Step II. Step III is the transmetalation reaction, in which the ligand transfers from one metal to another. The final reductive elimination (Step IV), leads to the formation of the final product and regeneration of the catalyst surface for the next cycle of reaction. The stability of our catalyst has been vindicated by recycling and detailed characterization (of the re-used catalyst), as discussed earlier, to facilitate the regeneration of the catalytic cycle.

Hence, our exceptional catalytic performance can be attributed to the close proximity and synergistic contact between Pd, Au NPs, and Brønsted basic sites from amine functional groups, thereby increasing the electron flux on Pd NPs under visible light irradiation conditions.^[50] The increased electron flux assisting in the C-X bond-breaking resulted in enhanced kinetics of the plasmon-mediated coupling reaction.

Conclusions

In conclusion, the effect of amine functionalization on the plasmonic catalysis of PdAu bimetallic NPs anchored within hierarchical zeotype materials was investigated. We observed that the tertiary amine functionalization was most efficient in influencing the reaction rate under visible light irradiation conditions. A reaction yield of 70% was observed in comparison to a 17% yield in dark conditions. An even higher product yield of 74%, under the monochromatic light ($\lambda = 550$ nm) irradiation conditions was observed, confirming the effect of Au LSPR in enhancing the rate of reaction. The enhanced catalytic reaction yield with tertiary amine was observed due to the following reasons; (i) efficient deposition of Pd NPs in close contact with Au and amine functional groups, (ii) enhanced Brønsted basicity of the catalytic system driving the reaction equilibrium in the forward direction and (iii) the formation of electron-rich Pd species, under light irradiation, due to the formation of hot charge carriers by Au and increased electron flux by Brønsted basic tertiary amine groups. The evidence of hot electron charge transfer has been observed in our preliminary SERS measurement analysis using PdAu/HP-AIPO-5-NR₃ nanostructured catalyst. Furthermore, the influence of versatile hierarchical support frameworks, in boosting the efficiency of the coupling reaction has also been probed. The present research work can foster new thoughts and further advancements in materials science and plasmon-mediated catalysis to design and discover new combinations and types of photocatalysts with enhanced quantum efficiency.

Experimental Section

Materials

Dimethyloctadecyl[(3-(trimethoxysilyl)propyl) ammonium chloride (DMOD), phosphoric acid (H_3PO_4 , 85% in H_2O), aluminium isopropoxide ($\text{Al}[\text{OCH}(\text{CH}_3)_2]_3$), triethylamine ($\text{N}(\text{CH}_2\text{CH}_3)_3$), palladium (II) acetate ($\text{Pd}(\text{OAc})_2$), tetrachloroauric (III) acid (HAuCl_4), ethanol ($\text{C}_2\text{H}_5\text{OH}$), biphenyl (C_6H_5)₂, phenylboronic acid ($\text{C}_6\text{H}_5\text{BO}_2$), naphthalene (C_{10}H_8), potassium carbonate (K_2CO_3) were purchased from Merck Chemicals. All chemicals were utilized as received without any additional purification.

Preparation of hierarchically porous aluminophosphate support, HP-AIPO-5

A large batch of hierarchically porous aluminophosphates (HP-AIPO-5) support material was synthesized as per the reported literature.^[14] The phosphoric acid (30.7 g) was diluted with distilled water (80 mL) and stirred for 5 min in a Teflon liner. To this, finely grounded aluminum isopropoxide (54.8 g) was slowly added to the stirring solution, followed by 40 mL of distilled water. The gel mixture was stirred continuously for 1.5 h. Subsequently, 18.95 g of DMOD solution followed by 21.6 g of triethylamine were dropwise added to the white gel along with 120 mL of water added and stirred for another 1.5 h. The gel was heated and stirred in a Parr reactor at 473 K for 24 h. The collected gel was centrifuged three times with water and dried overnight in an oven at 343 K. The white powder was then calcined at 873 K for 16 h under air, using a heating rate of 2.5 °C/min to produce HP-AIPO-5.

Synthesis of amine-functionalized HP-AIPO-5 (HP-AIPO-5-NR₃)

The mixture of HP-AIPO-5 (1.0 g) in toluene, along with the required amounts of amine functionalizing agent (5 mmol), [3-(diethylamino)propyl]trimethoxy silane, was stirred at 343 K for 20 h in an oil bath. The product was obtained by vacuum filtration and dried in an oven at 343 K overnight. The sample was labeled as HP-AIPO-5-NR₃ (or HP-AIPO-5-Amine-4) as tertiary amine was used for functionalization. Similarly, the HP-AIPO-5 support was also functionalized with other different amines by using silane agents such as (3-aminopropyl) trimethoxy silane, N-[3-(trimethoxysilyl)propyl]ethylenediamine and N¹-[3-(trimethoxysilyl)propyl]diethylenetriamine and labeled as HP-AIPO-5-Amine-1, HP-AIPO-5-Amine-2 and HP-AIPO-5-Amine-3, respectively. Scheme S1 shows the illustration for the preparation of amine-functionalized HP-AIPO-5 along with subsequent metal addition via a three-step synthesis strategy.

Synthesis of PdAu NPs on HP-AIPO-5-NR₃

The immobilization of PdAu bimetallic NPs was done by the step-wise synthesis method i.e., wet-impregnation method and LSPR-assisted deposition, leading to the uniform surface deposition of Pd on Au (according to Scheme S1). The functionalized HP-AIPO-5 was dispersed in 50 mL ethanol in a 100 mL glass reactor and ultrasonicated to make a clear suspension. Subsequently, the aqueous solution of HAuCl_4 was injected and stirred continuously for 4 h. The solvent was separated with rotavapor and the catalyst powder was dried in an oven for 8 h. The dried powdered sample was reduced under 5% H_2/N_2 mixture in a tube furnace for 4 h at 573 K to form metal NPs and labeled as Au/HP-AIPO-5-NR₃. The surface deposition of Pd on Au NPs was done by the LSPR-assisted deposition method under visible light irradiation. 0.5 g of Au/HP-AIPO-5-NR₃ was dispersed in water and irradiated under solar light

for 1 h, followed by the injection of Pd precursor solution. The solution was continuously stirred and irradiated for another 1 h, followed by filtration and drying in an oven at 343 K overnight. The obtained powder was then treated with 5% H_2/N_2 mixture in a tube furnace for 4 h at 573 K and labeled as PdAu/HP-AIPO-5-NR₃. Similar procedure was followed on blank HP-AIPO-5, and HP-AIPO-5-Amine-x (x = 1,2,3) support to form PdAu/HP-AIPO-5 and PdAu/HP-AIPO-5-Amine-x (x = 1,2,3), respectively.

Plasmon-mediated catalysis reaction

Suzuki-Miyaura coupling: The coupling reaction between iodobenzene and phenylboronic acid was done by preparing a solution of the powder catalyst in ethanol solvent. The powdered catalyst (50 mg), K_2CO_3 as mild base (124.5 mg), and phenylboronic acid (109.8 mg), were weighed in a glass reactor (50 mL). The ethanol (15 mL) was added to the reactor, and the coupling reaction was started by the addition of iodobenzene (1.0 mmol) via rubber septum. The reaction contents were stirred under solar light (Xe lamp) irradiation using a glass filter allowing wavelengths > 420 nm. The product formation was detected and calibrated using a Perkin Elmer Clarus 480 gas chromatograph. The set of reactions in the absence of light irradiation (dark conditions) were also performed.

Characterization

The absorption/transmission IR spectra were obtained by using a Perkin-Elmer FT-IR System 2000 spectrophotometer with a Hg-Cd-Te cryo-detector, available wavenumbers within the range 7200–580 cm^{-1} (resolution of 2 cm^{-1}). For the analysis of IR, self-supporting discs (~20 mg cm^{-2}) were used to compress the powder samples and then set in a stainless-steel cell (Aabspec). The thermal treatments were carried out in situ under vacuum or controlled atmosphere conditions. The simultaneous measurement of IR spectra at temperatures up to 873 K was obtained. Spectra were collected during outgassing at increasing temperature with steps of 50 K from room temperature to 573 K. Moreover, CO adsorption experiments were carried out at 77 K on samples previously outgassed at 573 K. Sample pre-treatment and CO adsorption were performed in a quartz IR cell equipped with KBr windows.

The Brunauer–Emmett–Teller (BET) specific surface area measurements were done by using a Micromeritics ASAP 2020 instrument at 77 K. Based on the amine stability, the pre-treatment of the samples was carried out in vacuum at 573 K for 2 h to remove the adsorbed impurities without compromising amine functionalization. Pore volumes and pore size distributions were calculated by the DTF method. The ICP analysis was done on a high-resolution inductively coupled plasma-mass spectrometer (MS) from Thermo Scientific ELEMENT 2XR (Waltham, MA, USA). The powder X-ray diffraction (XRD) spectra were obtained on Bruker D2 phaser diffractometer using $\text{Cu}_{\text{K}\alpha 1}$ radiation. The UV-vis spectra was obtained by Perkin Elmer Lambda 750S spectrophotometer in which BaSO_4 was used as a reference material. High-angle annular dark-field scanning transmission electron microscopy (HAADF-STEM) image was obtained from Sumika Chemical Analysis Service Ltd., Osaka, Japan. The TEM (transmission electron microscopy) measurements were performed using a side entry Jeol JEM 3010 (300 kV) microscope equipped with a LaB_6 filament and fitted with X-ray EDS analysis by a Link ISIS 200 detector. The sample preparation was done by depositing the powdered sample on a copper grid which was coated with a porous carbon film. An Ultrascan 1000 camera acquired all digital micrographs, and the processing was done by Gatan digital micrograph. The histograms of the metal NP size distribution were examined by observing a

minimum of 150 particles, and the mean diameter of the NP (d_m) was calculated by the following equation:

$$d_m = \frac{\sum d_i n_i}{\sum n_i}$$

where n_i is the number of NPs with diameter d_i .

The Pd K-edge and Au L₃-edge XAS measurements were carried out on the B18 beamline at the Diamond Light Source, UK. Supporting XAS measurements were also obtained from SPring-8, Hyogo, Japan. XPS measurements were performed at Harwell XPS, which is an EPSRC national facility in the UK.

The Clarus 480 GC (gas chromatograph) with a flame ionization detector and an Elite 5 column was employed to quantify the amount of product formation. The biphenyl was used as an external standard reagent. LOT LS0104 solar simulator fitted with a 150 W Xenon light source was employed to conduct reaction tests under visible light irradiation conditions.

Acknowledgements

This research work was by Grants-in-Aid for Scientific Research from the JSPS (Japan Society for the Promotion of Science) with grant numbers of 19K15311 and 22K21326. A part of the present work was supported by the Cooperative Research Program of the "Network Joint Research Center for Materials and Devices" with grant numbers of 20201097 and 20211069. Y. K., K. M., and H. Y. thank the Elements Strategy Initiative of MEXT [grant no. JP-MEXTP0112101003]. Priyanka Verma is grateful to the Royal Society for Newton International Fellowship (NIF\R1\180185) at the University of Southampton, UK, and to JSPS (P21042) for Postdoctoral fellowship at Osaka University, Japan. The authors thank the Diamond Light Source, Didcot, UK at B-18 beamline and SPring-8, Hyogo, Japan for XAS measurements. We also acknowledge EPSRC National Facility, HarwellXPS and National Oceanography Centre at University of Southampton for XPS and ICP analysis, respectively.

Conflict of Interest

The authors declare no conflict of interest.

Data Availability Statement

The data that support the findings of this study are available from the corresponding author upon reasonable request.

Keywords: amine functionalization · hierarchical porosity · plasmonic catalysis · visible-light irradiation

- [1] P. Verma, Y. Kuwahara, K. Mori, H. Yamashita, *Bull. Chem. Soc. Jpn.* **2019**, *92*, 19–29.
- [2] M. A. Mahmoud, *J. Phys. Chem. Lett.* **2014**, *5*, 2594–2600.
- [3] G. H. Chan, J. Zhao, E. M. Hicks, G. C. Schatz, R. P. Van Duyne, *Nano Lett.* **2007**, *7*, 1947–1952.
- [4] U. Aslam, V. G. Rao, S. Chavez, S. Linic, *Nat. Catal.* **2018**, *1*, 656–665.
- [5] P. Verma, K. Mori, Y. Kuwahara, R. Raja, H. Yamashita, *Mater Adv* **2021**, *2*, 880–906.
- [6] Z. Li, D. Kurouski, *Acc. Chem. Res.* **2021**, *54*, 2477–2487.
- [7] K. Mori, P. Verma, R. Hayashi, K. Fuku, H. Yamashita, *Chem. Eur. J.* **2015**, *21*, 11885–11893.
- [8] P. Verma, Y. Kuwahara, K. Mori, H. Yamashita, *J. Mater. Chem. A* **2015**, *3*, 18889–18897.
- [9] P. Verma, Y. Kuwahara, K. Mori, H. Yamashita, *J. Mater. Chem. A* **2016**, *4*, 10142–10150.
- [10] P. Verma, Y. Kuwahara, K. Mori, H. Yamashita, *Catal. Sci. Technol.* **2017**, *7*, 2551–2558.
- [11] P. Verma, Y. Kuwahara, K. Mori, H. Yamashita, *Chem. Eur. J.* **2017**, *23*, 3616–3622.
- [12] P. Verma, K. Yuan, Y. Kuwahara, K. Mori, H. Yamashita, *Appl. Catal. B* **2018**, *223*, 10–15.
- [13] P. Verma, M. Navlani-García, Y. Kuwahara, K. Mori, H. Yamashita, *J. Chem. Sci.* **2017**, *129*, 1661–1669.
- [14] S. H. Newland, W. Sinkler, T. Mezza, S. R. Bare, R. Raja, *Proc. R. Soc. A* **2016**, *472*, 20160095.
- [15] S. H. Newland, W. Sinkler, T. Mezza, S. R. Bare, M. Carravetta, I. M. Haies, A. Levy, S. Keenan, R. Raja, *ACS Catal.* **2015**, *5*, 6587–6593.
- [16] X. Y. Yang, L. H. Chen, Y. Li, J. C. Rooke, C. Sanchez, B. L. Su, *Chem. Soc. Rev.* **2017**, *46*, 481–558.
- [17] P. Verma, M. E. Potter, A. E. Oakley, P. M. Mhembere, R. Raja, *Nanomaterials* **2021**, *11*, 350.
- [18] X. Huang, Y. Li, Y. Chen, H. Zhou, X. Duan, Y. Huang, *Angew. Chem. Int. Ed.* **2013**, *52*, 6063–6067; *Angew. Chem.* **2013**, *125*, 6179–6183.
- [19] Q. Xiao, S. Sarina, E. Jaatinen, J. Jia, D. P. Arnold, H. Liu, H. Zhu, *Green Chem.* **2014**, *16*, 4272–4285.
- [20] S. Zhang, C. Chang, Z. Huang, Y. Ma, W. Gao, J. Li, Y. Qu, *ACS Catal.* **2015**, *5*, 6481–6488.
- [21] F. Wang, C. Li, H. Chen, R. Jiang, L. D. Sun, Q. Li, J. Wang, J. C. Yu, C. H. Yan, *J. Am. Chem. Soc.* **2013**, *135*, 5588–5601.
- [22] Y. Zhao, L. Du, H. Li, W. Xie, J. Chen, *J. Phys. Chem. Lett.* **2019**, *10*, 1286–1291.
- [23] C. Han, D. E. Gómez, Q. Xiao, J. Xu, *J. Catal.* **2021**, *397*, 205–211.
- [24] A. De Cattelle, A. Billen, W. Brullot, T. Verbiest, G. Koeckelberghs, *Appl. Organomet. Chem.* **2020**, *34*, 1–11.
- [25] G. Socrates, in *Infrared and Raman Characteristic Group Frequencies: Tables and Charts*, Wiley, UK, **2004**.
- [26] E. Gianotti, E. C. Oliveira, S. Coluccia, H. O. Pastore, L. Marchese, *Inorg. Chim. Acta* **2003**, *349*, 259–264.
- [27] E. Gianotti, E. C. Oliveira, S. Coluccia, H. O. Pastore, L. Marchese, in *Studies in Surface Science and Catalysis, Vol. 154* (Eds.: E. van Steen, M. Claeys, L. H. Callanan), Elsevier, **2004**, pp. 1498–1504.
- [28] M. Celebi, M. Yurderi, A. Bulut, M. Kaya, M. Zahmakiran, *Appl. Catal. B* **2016**, *180*, 53–64.
- [29] F. Liu, P. Zhang, *Appl. Phys. Lett.* **2010**, *96*, 2008–2011.
- [30] S. Alayoglu, P. Zavalij, B. Eichhorn, Q. Wang, A. I. Frenkel, P. Chupas, *ACS Nano* **2009**, *3*, 3127–3137.
- [31] A. Balerna, C. Evangelisti, E. Schiavi, G. Vitulli, L. Bertinetti, G. Martra, S. Mobilio, *J. Phys. Conf. Ser.* **2013**, *430*, 012052.
- [32] Z. Wang, S. Liang, X. Meng, S. Mao, X. Lian, Y. Wang, *Appl. Catal. B* **2021**, *291*, 120140.
- [33] S. Gao, W. Liu, C. Feng, N. Shang, C. Wang, *Catal. Sci. Technol.* **2016**, *6*, 869–874.
- [34] N. Miyauro, A. Suzuki, *Chem. Rev.* **1995**, *95*, 2457–2483.
- [35] B. Tao, D. W. Boykin, *J. Org. Chem.* **2004**, *69*, 4330–4335.
- [36] X. Guo, H. Dang, S. R. Wisniewski, E. M. Simmons, *Organometallics* **2022**, *41*, 1269–1274.
- [37] M. Khan, M. R. Shaik, S. F. Adil, M. Kuniyil, M. Ashraf, H. Frerichs, M. A. Sarif, M. R. H. Siddiqui, A. Al-Warthan, J. P. Labis, M. S. Islam, W. Tremel, M. N. Tahir, *Sci. Rep.* **2020**, *10*, 1–14.
- [38] K. Mori, Y. Futamura, S. Masuda, H. Kobayashi, H. Yamashita, *Nat. Commun.* **2019**, *10*, 4094.
- [39] K. Mori, S. Masuda, H. Tanaka, K. Yoshizawa, M. Che, H. Yamashita, *Chem. Commun.* **2017**, *53*, 4677–4680.
- [40] H. G. Soğukömeroğulları, Y. Karataş, M. Celebi, M. Gülcan, M. Sönmez, M. Zahmakiran, *J. Hazard. Mater.* **2019**, *369*, 96–107.
- [41] A. Matsuo, S. Hasegawa, S. Takano, T. Tsukuda, *Langmuir* **2020**, *36*, 7844–7849.
- [42] D. Han, Z. Bao, H. Xing, Y. Yang, Q. Ren, Z. Zhang, *Nanoscale* **2017**, *9*, 6026–6032.
- [43] S. Rohani, A. Ziarati, G. M. Ziarani, A. Badiei, T. Burgi, *Catal. Sci. Technol.* **2019**, *9*, 3820–3827.

- [44] J. Guo, Y. Zhang, L. Shi, Y. Zhu, M. F. Mideksa, K. Hou, W. Zhao, D. Wang, M. Zhao, X. Zhang, J. Lv, J. Zhang, X. Wang, Z. Tang, *J. Am. Chem. Soc.* **2017**, *139*, 17964–17972.
- [45] X. Zhu, H. Jia, X. M. Zhu, S. Cheng, X. Zhuo, F. Qin, Z. Yang, J. Wang, *Adv. Funct. Mater.* **2017**, *27*, 1–15.
- [46] Q. Xiao, S. Sarina, E. Jaatinen, J. Jia, D. P. Arnold, H. Liu, H. Zhu, *Green Chem.* **2014**, *16*, 4272–4285.
- [47] H. S. Feng, F. Dong, H. S. Su, M. M. Sartin, B. Ren, *J. Appl. Phys.* **2020**, *128*, 173105.
- [48] T. T. Trinh, R. Sato, M. Sakamoto, Y. Fujiyoshi, M. Haruta, H. Kurata, T. Teranishi, *Nanoscale* **2015**, *7*, 12435–12444.
- [49] B. Zhang, J. Song, H. Liu, J. Shi, J. Ma, H. Fan, W. Wang, P. Zhang, B. Han, *Green Chem.* **2014**, *16*, 1198–1201.
- [50] J. Han, Z. Zhang, Z. Hao, G. Li, T. Liu, *J. Colloid Interface Sci.* **2021**, *587*, 736–742.

Manuscript received: September 30, 2022
Revised manuscript received: December 22, 2022
Accepted manuscript online: January 3, 2023
Version of record online: January 16, 2023